Carbon 142 (2019) 131–140

Contents lists available at ScienceDirect

Carbon

journal homepage: www.elsevier.com/locate/carbon

Trace electrosprayed nanopolystyrene facilitated dispersion of multiwalled carbon nanotubes: Simultaneously strengthening and toughening epoxy

Hongbo Gu [a, *], Hongyuan Zhang [a], Chao Ma [a], Xiaojiang Xu [a], Yaqing Wang [a], Zicheng Wang [b, c], Renbo Wei [c, **], Hu Liu [b, d], Chuntai Liu [d], Qian Shao [e], Xianmin Mai [f, ***], Zhanhu Guo [b, ****]

[a] Key Lab of Chemical Assessment and Sustainability, Department of Chemistry, Tongji University, Shanghai, 200092, People's Republic of China
[b] Integrated Composites Laboratory (ICL), Department of Chemical & Biomolecular Engineering, University of Tennessee, Knoxville, TN, 37966, USA
[c] Research Branch of Advanced Functional Materials, School of Materials and Energy, University of Electronic Science and Technology of China, Chengdu, 611731, PR China
[d] Key Laboratory of Materials Processing and Mold (Zhengzhou University), Ministry of Education, National Engineering Research Center for Advanced Polymer Processing Technology, Zhengzhou University, Zhengzhou, 450002, China
[e] College of Chemical and Environmental Engineering, Shandong University of Science and Technology, Qingdao, Shandong, 266590, China
[f] School of Urban Planning and Architecture, Southwest Minzu University, Chengdu, 610041, China

ARTICLE INFO

Article history:
Received 13 September 2018
Received in revised form
7 October 2018
Accepted 8 October 2018
Available online 12 October 2018

Keywords:
Multi-walled carbon nanotubes
Nanopolystyrene
Epoxy nanohybrids
Mechanical properties
Electrical conductivity

ABSTRACT

The search of multifunctional epoxy nanocomposites with both strength and toughness combined with smart features such as electrical conductivity is essential in design of advanced materials. In this work, by utilizing a binary nanofiller strategy, both strength and toughness as well as high electrical conductivity are obtained in epoxy with trace nanopolystyrene grafted with epichlorohydrin (nano *g*-PS) to facilitate the dispersion of multi-walled carbon nanotubes (MWCNTs). The increased tensile strength (37.6%) and flexural strength (34.4%) are acquired in nano *g*-PS (0.0677 vol%)/MWCNTs (0.0335 vol%)/epoxy in contrast to pure epoxy. A remarkably improved tensile toughness up to 379.2% and an increased elongation at break up to 208.3% are obtained in this epoxy nanohybrid. The synergistic interactions among nano *g*-PS, MWCNTs and epoxy matrix as well as the state transition of nano *g*-PS from glassy state to fluid state provide an improved dispersion of nanofillers which is responsible for the increased electrical conductivity and enhanced mechanical properties. The decreased surface resistivity allows these nanohybrids to sufficiently dissipate surface charges as an antistatic material. This work provides an effective way to disperse carbon nanotubes with small amount of thermoplastic PS to simultaneously strengthen and toughen the thermosetting epoxy while introducing highly conductive function.

1. Introduction

Epoxy, as one of the most popular engineering thermosets, has been widely applied in the fields of adhesive, automobile, coatings, marine and electronics [1–9]. With the rapid development of electronics, automobile and aerospace vector, as an electrical insulating material, epoxy with relatively high electrical conductivity is required for effective electrostatic dissipation [10]. Therefore, a lot of efforts have been dedicated to enhance both mechanical properties and electrical properties of epoxy. Numerous nanofillers with various dimensions such as 0D (e.g. nanoparticles) [11,12], 1D (e.g. carbon nanotubes (CNTs) [13–17], carbon nanofibers (CNFs) [18,19]), 2D (i.e. graphene) [20], 3D (e.g. 3D graphene foam [21], and 3D CNT sponge [22]) have been introduced into the polymer matrix to form nanocomposites. However, most of these nanofillers required a relatively higher loading (for example, 2.7 vol% of functionalized graphene oxide

* Corresponding author.
** Corresponding author.
*** Corresponding author.
**** Corresponding author.
E-mail addresses: hongbogu2014@tongji.edu.cn (H. Gu), weirb10@uestc.edu.cn (R. Wei), maixianmin@foxmail.com (X. Mai), zguo10@utk.edu (Z. Guo).

https://doi.org/10.1016/j.carbon.2018.10.029
0008-6223/

(GO) [23] and 5.0 wt% of CNTs [24]), which obviously increased the cost and reduced the processibility of epoxy.

Owing to high Young's modulus (0.32–1.47 TPa), high strength (10–52 GPa), and toughness around 770 J g^{-1} [25] together with exceptional electrical properties and thermal conductivity [26,27], CNTs exhibit many advantages in the fabrication of multifunctional epoxy nanocomposites with high electrical and thermal conductivity. However, the lack of surface functional groups and easy entanglement due to high surface energy [28] are detrimental to attain desired mechanical, electrical, thermal and other properties [29]. In order to obtain optimum dispersion of CNTs within epoxy matrix and better compatibility between epoxy and CNTs, chemical modification including both covalent and noncovalent functionalization of CNTs is normally used before mixing with epoxy matrix [30]. Generally, covalent functionalization is related to the formation of fucntional groups on the surface of CNTs such as carboxylic groups (–COOH) [31], amine groups (–NH_2) [32], hydroxyl groups (–OH) [33], etc. and noncovalent functionalization involves attaching the target fucntional groups on the surface of CNTs (e.g. polypyrole (PPy) [34], polyaniline (PANI) [35], etc.). Although surface functionalization could boost the interaction between CNTs and epoxy matrix, most of these chemical methods might damage the chemical structure of CNTs during the modification process, leading to the formation of defects and hindering the electrical and thermal conductivity in CNTs [36]. For example, Gu et al. [37] used PANI as a coupling agent between multi-walled CNTs (MWCNTs) and epoxy, in which the tensile strength was increased by 85% compared with pure epoxy, however, the volume resistivity of MWCNTs/epoxy was still around 10^{11} Ω cm. Recently, distinctly different binary nanofillers method has been introduced as the nanoreinforcements to the epoxy matrix. For instance, Liu et al. [38] utilized clay as an additional additive to improve the disersion quality of single walled CNTs (SWCNTs) in epoxy matrix, in which both electrical and mechanical properties were enhanced. Gu et al. [39] applied nanomagnetite into CNFs/epoxy nanocomposites, and reported not only significantly reduced resistivity (10^2 Ω cm), but also strengthened nanomagnetite/CNFs/epoxy nanohybrids. Unfortunately, the nanoreinforcement mechanism is still unknown. The understanding of reinforcement mechanism is essential for the design of epoxy nanohybrid structures and industrial applications [40].

The demand for advanced materials with both strength and toughness is imperative, especially for engineering epoxy. Although high crosslinking degree endows epoxy with superior mechanical properties such as high tensile strength and Young's modulus, the intrinsic brittleness and poor fracture toughness [41] arising from internal stresses produced during curing process and restricted crack growth from plastic deformation [42] severely limit its applications in the aerospace, automobile, and marine systems as a structural conterpart [43]. Normally, strength and toughness contradict each other since the strength describes a resistance of material to non-recoverable deformation while the toughness is related to the energy required for dissipating local high stress to cause the fracture [44]. Recently, thermoplastic materials such as poly(ether ether ketone) with pendent methyl group (PEEKM) [45], poly(ethyleneoxide)-poly-(ethylene-alt-propylene) (PEO-PEP) block copolymer [46] have gained more attentions for toughning epoxy, in which the typically required high loading of this tougher (5–20 wt%) might result in an apparent reduced mechanical properties [47]. Even though the aminated polystyrene (PS) [48] and epoxide grafted PS [49] have been reported to increase both tensile strength and toughness of epoxy, the insulating nature of these materials also restricts applications of epoxy in the electronic devices.

In this work, we developed a nanosized PS particles grafted with epichlorohydrin (ECH) through electrospraying to manufacture epoxy nanohybrids with binary nanofillers of trace nanosized PS grafted with ECH and MWCNTs without using any chemical treatments. By simply applying this design, a 37.6% enhancement of ultimate tensile strength and a 34.4% increase in ultimate flexural strength are attained in the trace nano PS grafted with ECH (0.0677 vol%)/MWCNTs (0.0335 vol%)/epoxy nanohybrids. Furthermore, a 279.2% improvement in tensile toughness and a 108.3% increase in the elongation at break are achieved in these epoxy nanohybrids relative to pure epoxy. This nanoreinforcement mechanism is explored considering the synergistic interactions among nano PS grafted with ECH, MWCNTs and epoxy matrix as well as the state transition of nano PS grafted with ECH from galssy state to fluid state, and major strain distribution.

2. Experimental

2.1. Fabrication of nano g-PS/MWCNTs/epoxy nanohybrids

Fig. 1 shows the preparation procedure of nano *g*-PS/MWCNTs/epoxy nanohybrids. Firstly, the PS (Taizhou Suosi education equipment Co., Ltd.) was firstly grafted with epichlorohydrin (*g*-PS) following the procedures as reported in a previous work [49] in order to increase the compatibility between *g*-PS and epoxy matrix. Then the 5.0 wt% loading of *g*-PS/DMF (Sinopharm Chemical Reagent Co., Ltd.) solution was electrosprayed to obtain the nano *g*-PS particles. After that, the nano *g*-PS particles and MWCNTs (Sigma Aldrich) were mixed with epon 862 epoxy resin (bisphenol F epoxy, Hexion Inc.) under mechanically stirred with sonication. The curing agent EK3402 (Hexion Inc.) was added into the above mixture with a resin/curing agent weight ratio of 100/26.5 following a mechanical stirring and sonication. After increasing temperature to 50 °C, the well dispersed suspensions were poured into a silicon rubber mold and cured at 120 °C for 5 h. Finally, the nano *g*-PS/MWCNTs/epoxy nanohybrids were obtained after cooling down to room temperature naturally. In comparison, the pure epoxy, the epoxy nanocomposites with 0.0677 vol% of *g*-PS, and the epoxy nanocomposites with 0.0067, 0.0101, 0.0104, 0.0111, 0.0201, 0.0335, 0.0435, 0.0502, 0.0670, 0.0837 vol% of MWCNTs were also synthesized following the same procedures without adding *g*-PS or MWCNTs. The detailed experimental is mentioned in the supporting information.

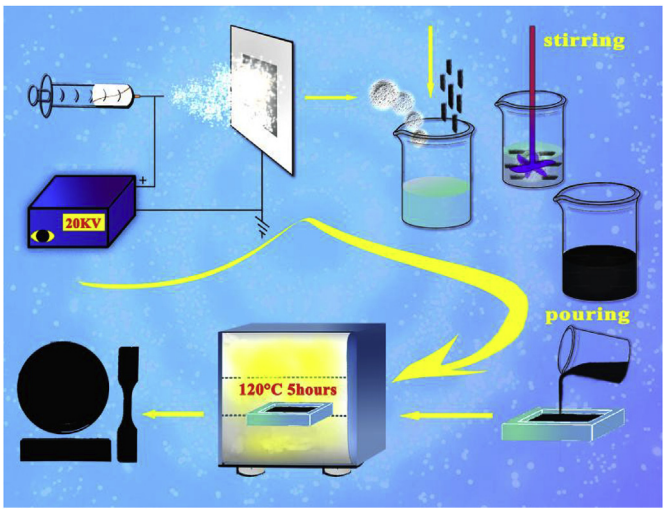

Fig. 1. Preparation procedure of nano *g*-PS/MWCNTs/epoxy nanohybrids. (A colour version of this figure can be viewed online.)

2.2. Characterizations

The electrical conductivity and surface resistivity of MWCNTs/epoxy nanocomposites and epoxy nanohybrids were measured by the DC resistance along the disc samples with a diameter of appropriate 60 mm with a HEST-200 high resistant meter from Beijing Huace Testing Instrument Co., Ltd. at room temperature. The reported values were the average value of three valid measurements with a deviation less than 10%. The tensile tests and three point bending tests were performed using a dog-bone shaped sample with the American Society for Testing and Materials (ASTM, standard D412-98a, 2002) and a typical rectangular sample with dimension of $60 \times 10 \times 3\ mm^3$ following the ASTM standard D5023-15 (2015) in a unidirectional tensile test machine (Shanghai Xieqiang Instrument Technology Co. Ltd.) at room temperature, respectively. A 3D motion and deformation sensor ARAMIS system with GOM Correlate software from GOM GmbH was conducted on the dog-bone shaped samples to record the real-time stress-strain characteristics. Other detailed characterizations please see supporting information.

3. Results and discussion

Firstly, with the purpose of increasing the compatibility of PS with epoxy matrix, the as-received PS was chemically grafted with ECH to form the ECH grafted PS (*g*-PS). After that, the *g*-PS was electrosprayed into nano *g*-PS particles *via* a 5.0 wt% *g*-PS dimethylformamide (DMF) solution. As shown in SEM images, Figs. S2A and S2B, the electrosprayed *g*-PS particles are particulate with a diameter around 80–180 nm measured by Nano Measurer software. With the evaporation of DMF after electrospraying process, some of the *g*-PS particles stick together and form particles with size bigger than 200 nm. The evident broad peak within the wavenumber range from 3100 to 3700 cm^{-1} in the FTIR spectrum of nano *g*-PS (Figs. S2C–b) compared to the FTIR spectrum of as-received PS (Figs. S2C–a) arises from the O–H stretching vibration [50]. The nano *g*-PS has an obvious degradation from 200 to 300 °C in contrast with the as-received PS, Figs. S2D–b and Figs. S2D–a, respectively, which is due to the degradation of C–O–C group in the nano *g*-PS as reported in the literature [51,52]. Compared with the deconvoluted high resolution C1s XPS spectrum of as-received PS, Fig. S2E, the nano *g*-PS owns two more binding energy peaks located at 286.1 and 287.0 eV, corresponding to the C–OH and C–O–C, accordingly [53,54]. All of these results confirm the existence of hydroxyl and epoxide groups on the polymer backbone of nano *g*-PS. Owing to the chemical reaction and similar polarity, both hydroxyl and epoxide groups have the affinity with epoxy matrix.

Subsequently, epoxy nanocomposites filled with different loadings of MWCNTs from 0.0067 to 0.0837 vol% were prepared in order to obtain the percolation threshold. The obtained percolation curve of MWCNTs/epoxy nanocomposites is plotted in Fig. 2. The electrical conductivity of MWCNTs/epoxy nanocomposites displays a dramatic change around 7 orders of magnitudes (from 10^{-13} to $10^{-6}\ S\ m^{-1}$), which is normally induced by the formation of percolation network [55]. The percolation threshold (ϕ_c) can be computed by percolation theory from eq (1) [56]:

$$\sigma = \sigma_0(\phi - \phi_c)^t \quad (1)$$

where σ is the electrical conductivity of the MWCNTs/epoxy nanocomposites, σ_0 is a constant, t represents the electrical conductivity exponent that is generally used to express the dimensionality of the system with values typically around ~1.3 and ~2.0 for two and three-dimensions, respectively [57]. By fitting the

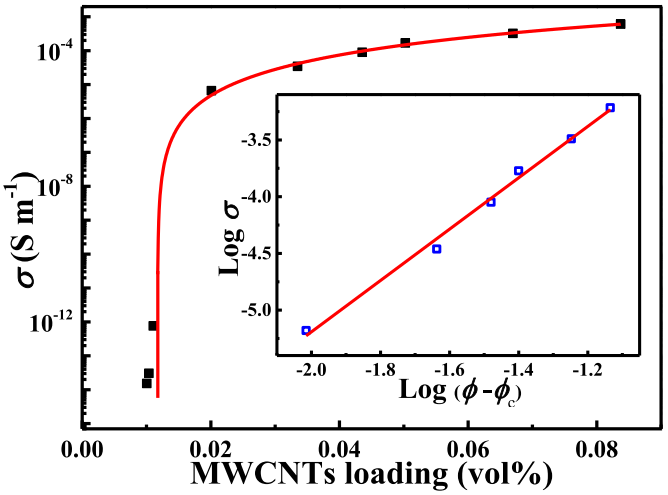

Fig. 2. Electrical conductivity as a function of MWCNTs loading. (A colour version of this figure can be viewed online.)

percolation curve with this equation, the estimated ϕ_c for the MWCNTs/epoxy nanocomposites is 0.0117 vol%. As displayed in the inset of Fig. 2, t is calculated to be 2.26, suggesting a complex electrical conducting network in the MWCNTs/epoxy nanocomposites. Though the percolation threshold of MWCNTs/epoxy is pretty low, the scarcity of functional groups on the surface of MWCNTs and aggolomeration may severely lower the mechanical property of epoxy matrix. Therefore, our as-prepared electrosprayed nano *g*-PS is introduced into MWCNTs/epoxy to form a ternary epoxy nanohybrids, aiming to facilitate the dispersion of MWCNTs within epoxy matrix and strengthen the mechanical property of epoxy matrix. As aforementioned in Fig. 2, the electrical conductivity for 0.0335 vol% of MWCNTs/epoxy nanocomposites is one order of magnitude higher than that of 0.0201 vol% MWCNTs/epoxy nanocomposites. After further increasing the loading of MWCNTs, the electrical conductivity has only a little bit change, whereas the tensile strength is decreased significantly, Fig. S3 (which is a typical example for the scaling law of strength and toughness of epoxy: materials with lower strength have a tendency to be tougher). Considering processibility, mechanical properties, and electrical conductivity of MWCNTs/epoxy nanocomposites, 0.0335 vol% loading of MWCNTs/epoxy nanocomposites was chosen to prepare nano *g*-PS/MWCNTs (0.0335 vol%)/epoxy nanohybrids with different loadings of nano *g*-PS to investigate their properties in the following. The obtained electrical conductivity of nano *g*-PS (0.0193–0.1160 vol%)/MWCNTs (0.0335 vol%)/epoxy nanohybrids is illustrated in Fig. S4. With adding nano *g*-PS into MWCNTs/epoxy nanocomposites, the electrical conductivity for all the nano *g*-PS (varying from 0.0193 to 0.1160 vol%)/MWCNTs (0.0335 vol%)/epoxy nanohybrids is higher than that of MWCNTs (0.0335 vol%)/epoxy nanocomposites. Particularly, nano *g*-PS (0.0677 vol%)/MWCNTs (0.0335 vol%)/epoxy nanohybrid possesses the highest electrical conductivity, which is one order of magnitude higher than that of MWCNTs (0.0335 vol%)/epoxy nanocomposites with same loading of MWCNTs.

The typical stress-strain curves of pure epoxy, MWCNTs (0.0335 vol%)/epoxy, nano *g*-PS/epoxy, and nano *g*-PS (0.0193–0.1160 vol%)/MWCNTs (0.0335 vol%)/epoxy nanohybrids are displayed in Fig. 3A and Fig. S6A, and the corresponding tensile properties including tensile strength, Young's modulus, and the elongation at break are summarized in Table 1. In the stress-strain curve of pure epoxy, no noticeable plastic deformation is observed before fracture, presenting a representative brittle failure. In

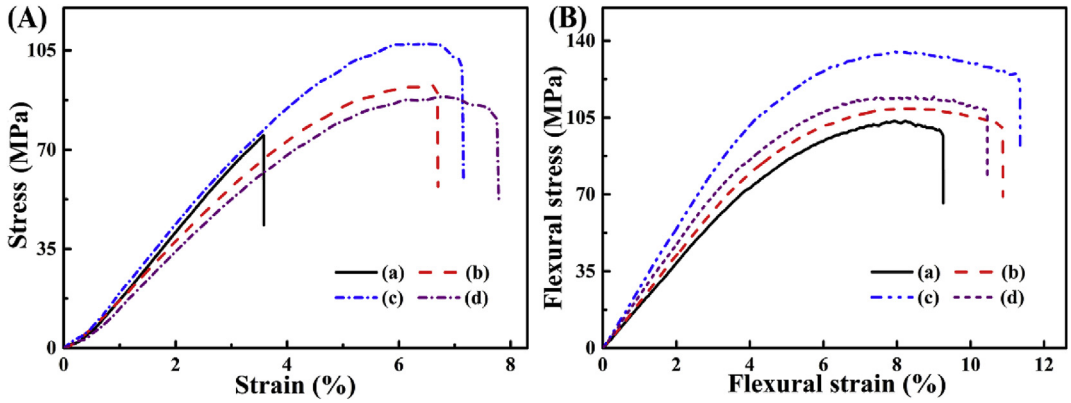

Fig. 3. (A) Stress-strain curves of (a) pure epoxy, (b) MWCNTs (0.0335 vol%)/epoxy, (c) nano *g*-PS (0.0677 vol%)/MWCNTs (0.0335 vol%)/epoxy, and (d) nano *g*-PS (0.0677 vol %)/epoxy; (B) flexural stress-flexural strain curves of (a) pure epoxy, (b) MWCNTs (0.0335 vol%)/epoxy, (c) nano *g*-PS (0.0677 vol%)/MWCNTs (0.0335 vol%)/epoxy, and (d) nano *g*-PS (0.0677 vol%)/epoxy. (A colour version of this figure can be viewed online.)

Table 1
Tensile mechanical properties of pure epoxy and epoxy nanohybrids.

Sample (vol%)	Ultimate tensile strength (MPa)	Young's modulus (GPa)	Elongation at break (%)	Modulus of toughness U_t, (MJ m^{-3} or MPa)
Pure Epoxy	77.6 ± 0.7	2.4 ± 0.1	3.6 ± 0.1	128.7
0.0335 MWCNTs	92.1 ± 1.5	2.1 ± 0.1	6.7 ± 0.4	337.8
0.0193–0.0335	97.3 ± 1.5	2.2 ± 0.1	7.1 ± 0.4	417.6
0.0483–0.0335	98.5 ± 1.7	2.2 ± 0.1	6.8 ± 0.5	410.6
0.0677–0.0335	106.5 ± 0.8	2.3 ± 0.1	7.0 ± 0.3	488.0
0.0773–0.0335	98.0 ± 1.2	2.0 ± 0.1	7.2 ± 0.2	406.3
0.0966–0.0335	95.9 ± 1.8	2.1 ± 0.1	7.5 ± 0.2	446.4
0.1160–0.0335	90.6 ± 1.9	2.1 ± 0.1	7.4 ± 0.2	426.9
0.0677 nano *g*-PS	89.3 ± 1.5	2.0 ± 0.1	8.1 ± 0.4	446.8

contrast, after utilizing nano *g*-PS into 0.0335 vol% loading of MWCNTs/epoxy, a noticeable extensive plastic deformation occurs before fracture in their stress-strain curves, Fig. 3A–c, pointing out a ductile failure feature. Moreover, the average ultimate tensile strength of nano *g*-PS/MWCNTs/epoxy nanohybrids increases with increasing the nano *g*-PS loading to 0.0677 vol% and then decreases with further increasing the nano *g*-PS loading, Fig. S6(B). Especially, the average ultimate tensile strength for the nano *g*-PS (0.0677 vol %)/MWCNTs (0.0335 vol%)/epoxy nanohybrids (106.5 MPa) is obviously improved by 37.6, 15.6, and 16.6% relative to that of pure epoxy (77.6 MPa), MWCNTs (0.0335 vol%)/epoxy nanocomposites (92.1 MPa) and nano *g*-PS (0.0677 vol%)/epoxy nanocomposites (91.3 MPa), respectively, The Young's modulus of nano *g*-PS/MWCNTs/epoxy nanohybrids has no obvious change compared with pure epoxy (around 2.4 GPa), MWCNTs/epoxy nanocomposites and nano *g*-PS/epoxy nanocomposites, which may be due to the trace binary fillers of MWCNTs (0.0335 vol%) and nano *g*-PS (0.0193–0.1160 vol%). The Young's modulus is normally related to the stiff interfacial layer between nanofillers and epoxy matrix. The 0.0335 vol% loading of MWCNTs is not sufficient enough to change the elastic property of epoxy [49]. However, it's worth mentioning that the elongation at break for all the nano *g*-PS/MWCNTs/epoxy nanohybrids (around 6.8–7.5%) is much longer (which is almost 88.9–108.3% increase) than that of pure epoxy (3.6%), manifesting an evident toughening effect after adding the nano *g*-PS into MWCNTs/epoxy nanocomposites. The modulus of toughness (U_t) calculated from the area under the stress-strain curve, as an indicator of fracture toughness parameter [39], is also listed in Table 1. It's noticed that the U_t for all of nano *g*-PS/MWCNTs/epoxy nanohybrids is much higher than that of pure epoxy (128.7 MJ m^{-3}) and MWCNTs (0.0335 vol%)/epoxy nanocomposites (337.8 MJ m^{-3}). Especially, for the nano *g*-PS (0.0677 vol %)/MWCNTs (0.0335 vol%)/epoxy nanohybrids, the U_t is 279.2 and 44.5% higher than that of pure epoxy and MWCNTs (0.0335 vol %)/epoxy nanocomposites, accordingly, demonstrating a brilliantly improved tensile fracture toughness as a verification of irreplaceable role of nano *g*-PS in the nano *g*-PS (0.0677 vol%)/MWCNTs (0.0335 vol%)/epoxy nanohybrids for the enhancement of tensile strength.

The flexural properties of pure epoxy, MWCNTs (0.0335 vol %)/epoxy, nano *g*-PS (0.0677 vol%)/epoxy, and nano *g*-PS (0.02–0.12 wt%)/MWCNTs (0.0335 vol%)/epoxy nanohybrids were also studied through the three-point bending test. The corresponding flexural stress-flexural strain curves are depicted in Fig. 3B and Fig. S6C. The obtained flexural properties of these materials are summarized in Table S1. The Young's modulus from tensile tests normally describes the stiffness of a solid material, whereas the flexural modulus is an intensive property of a material which expresses a tendency for a material to resist the bending in the flexural deformation [58]. In this work, the flexural modulus for nano *g*-PS (0.0193–0.1160 vol%)/MWCNTs (0.0335 vol %)/epoxy nanohybrids (2.0–2.6 GPa) is a little higher than that of pure epoxy (1.9 GPa). The average ultimate flexural strength for pure epoxy, MWCNTs (0.0335 vol%)/epoxy, and nano *g*-PS (0.0677 vol%)/epoxy is 104.5, 110.6, and 119.1 MPa, respectively. Similar to the tensile properties, the average ultimate flexural strength is increased with increasing the nano *g*-PS loading to 0.0677 vol% and then decreased as nano *g*-PS loading increases further, Fig. S6D. The improved ultimate flexural strength for the nano *g*-PS (0.0677 vol%)/MWCNTs (0.0335 vol%)/epoxy nanohybrids (140.5 MPa) is respectively 34.4, 27.0, and 18.0% higher than that of pure epoxy, MWCNTs (0.0335 vol%)/epoxy, and nano *g*-PS (0.0677 vol%)/epoxy. Both tensile test and three-point bending test results signify that adding nano *g*-PS into

MWCNTs/epoxy could effectively produce the reinforced and toughened epoxy nanohybrids. The mechanical properties of our nano *g*-PS/MWCNTs/epoxy nanohybrids and the reported values are compared and listed in Table 2. It turns out that the mechanical properties including flexural strength and tensile strength are higher than most of reported values, especially for the tensile toughness. Although some reported values are higher than our results, the content of nanofillers in our epoxy nanohybrids is less than these values, which is beneficial for manufacturing.

With the purpose of investigating exceptional mechanical properties of nano *g*-PS/MWCNTs/epoxy nanohybrids, the fracture surface after tensile tests and the dispersion quality of these epoxy nanohybrids were carried out, Fig. 4. In the SEM microstructures of fracture surface for pure epoxy, Figure S7A and S7B, a smooth fracture surface with "river-like" patterns is acquired as expected, signifying a representative brittle failure structure resulting from the rapid crack propagation [59], the same as indicated in the stress-strain curve, Fig. 3A–a. However, as a consequence of fracture energy dissipation, after applying nano *g*-PS and MWCNTs into epoxy, the fracture surface of these nanocomposites becomes relatively rough. Normally, rough fracture surface is from the inhibition of crack propagation and energy dissipation by the existence of nanofillers [60]. In the SEM image for the fracture surface of nano *g*-PS (0.0677 vol%)/epoxy nanocomposites, Fig. 4A, the small holes from the dispersed nano *g*-PS in the epoxy matrix are obviously observed in Fig. 4B. Evidently, in the MWCNTs (0.0335 vol %)/epoxy nanocomposites, Fig. 4C, the MWCNTs are severely aggolomerated on the fracture surface, which may serve as the crack initiators when the external tensile force is applied to the epoxy nanocomposites and causes the decreased tensile strength. In addition, there are many holes surrounded MWCNTs as indicated by the blue circle, Fig. 4D, demonstrating a poor adhesion between MWCNTs and epoxy. By contrast, in the SEM image for the fracture surface of nano *g*-PS (0.0677 vol%)/MWCNTs (0.0335 vol%)/epoxy nanohybrids, Fig. 4E and Fig. S8, many new fracture surfaces are formed accompanied with more dimples appeared, which could help dissipate more energies (called extrinsic toughening, which could effectively resist the crack growth [61]), leading to ductile failure and increased tensile strength. Moreover, it's worth noting that the observed many white dots as shown in the blue circle, Fig. 4F, indicate well dispersed instead of aggolomerated MWCNTs. Interestingly, the holes observed in Fig. 4D disappear. Instead, the MWCNTs tightly stick to the epoxy matrix, suggesting that after adding nano *g*-PS into epoxy matrix, the synergistic interaction among nano *g*-PS, MWCNTs and epoxy matrix could eliminate the agglomeration of MWCNTs, leading to a better dispersion quality of nanofillers and enhanced mechanical properties.

In order to further evaluate the dispersion quality of MWCNTs in the epoxy nanohybrids, the TEM micrographs of MWCNTs (0.0335 vol%)/epoxy nanocomposites and nano *g*-PS (0.0677 vol %)/MWCNTs (0.0335 vol%)/epoxy nanohybrids were performed and shown in Figs. S9A and S9B. Notably, the as-received MWCNTs are agglomerated in the epoxy matrix, Fig. S9B, which is consistent with SEM image, Fig. 4D, whereas the MWCNTs are well distributed in the epoxy matrix after introducing nano *g*-PS into MWCNTs (0.0335 vol%)/epoxy nanocomposites, Fig. S9A. Normally, there are two methods to increase the interaction between nanofillers and epoxy matrix and facilitate the dispersion of nanofillers within epoxy matrix. One is weak physical method of adding polymers through van der Waals forces, hydrogen bonding, electrostatic, steric interaction, and Lewis acid-base interactions, which could diminish the voids between nanofillers and matrix and increase the mechanical properties. The other is to use the strong chemical covalent bonding between nanofillers and matrix [1]. In this work, both methods might be responsible for the improved mechanical property. On one hand, the chemically grafted nano *g*-PS with hydroxyl and epoxide groups could increase the chemical covalent bonding between nano *g*-PS and epoxy matrix as confirmed in our previous reported work [49]. On the other hand, the presence of nano *g*-PS could improve the dispersion quality of MWCNTs within epoxy matrix and further result in the enhanced mechanical properties in the nano *g*-PS/MWCNTs/epoxy nanohybrids.

With the aim of exploring this reinforcement phenomenon, a 3D Motion and Deformation sensor ARAMIS system (GOM GmbH), which is a perfect tool to provide an optimum understanding of the component behavior, was employed to monitor the real-time stress-strain variations and the whole process was recorded in the video program of SI. Fig. 5 depicts the 3D major strain distribution images of pure epoxy, MWCNTs (0.0335 vol%)/epoxy, nano *g*-PS (0.0677 vol%)/epoxy and nano *g*-PS (0.0677 vol%)/MWCNTs (0.0335 vol%)/epoxy nanohybrids for the moment before fracture during the tensile process. As shown in 3D major strain distribution images, under the external stress, the color varies with changing the strain at different locations as marked on the right side of each 3D major strain distribution image. The red denotes the highly concentrated major strain. Normally, when the highly concentrated major strain is achieved, the sample starts to fracture. For pure epoxy, Fig. 5A, the major strain is highly concentrated to the middle of dog-bone shaped sample and then the sample begins to fracture. For the MWCNTs (0.0335 vol%)/epoxy nanocomposites, the major

Table 2
Improvement of mechanical properties for epoxy nanocomposites with different fillers.

Fillers	Content	Flexural Strength	Tensile Strength	Tensile Toughness
CNT sponge [22]	0.66 wt%	102%	64%	250%
MWCNTs-COOH [78]	1 wt%	22%		
Amino-DWCNT [79]	0.5 wt%	–	8.6%	43%
Functionalized graphene nanoplatelates [80]	0.1 wt%	22%	–	–
3D graphene skeleton [81]	0.2 wt%	43.2%	120.9%	–
3D graphene aerogel [82]	1.4 wt%	2%	–	64%
Amino-graphene nanoplatelates [83]	1 wt%	–	21%	82%
Epoxide-polystyrene [49]	1.5 wt%	–	25.5%	176.6%
Aminated polystyrene [48]	15 wt%	–	25.6%	84.3%
Fe_3O_4/Carbon nanofibers [39]	10 wt%/2.5 wt%	–	26.2%	137.83%
Poly(acrylonitrile-co-butadiene-co-styrene)/clay [84]	4 wt%/2.5 wt%	–	45%	–
Cloisite 25A/poly(ether ether ketone) [85]	1 wt%/5 wt%	−9.8%	3.2%	37.1%
Montmorillonite/polyamide [86]	2 wt%/20 wt%	–	–	80%
Nano g-PS/MWCNTs[a]	***0.07 wt%/0.1 wt%***[b]	***34.4%***	***37.6%***	***279.2%***

[a] This work.
[b] The corresponding weight percentage for our as-prepared nano g-PS (0.0677 vol%)/MWCNTs (0.0355 vol%). We used volume percent to express the content of our nanofillers since the percolation threshold was obtained from the volume percent.

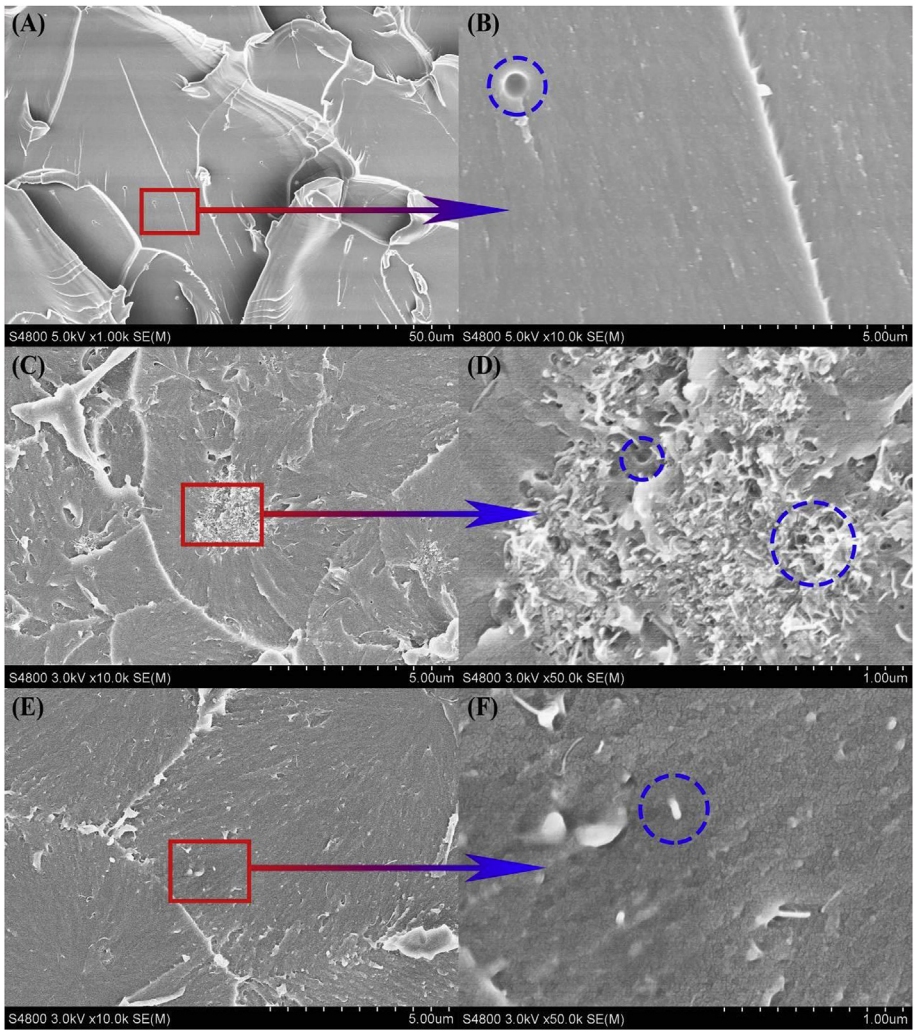

Fig. 4. SEM microstructures of fracture surface (A) nano *g*-PS (0.0677 vol%)/epoxy, (C) MWCNTs (0.0335 vol%)/epoxy, and (E) nano *g*-PS (0.0677 vol%)/MWCNTs (0.0335 vol%)/epoxy nanohybrids. (B), (D) and (F) are corresponding (A), (C), and (E) SEM images at high magnification. (A colour version of this figure can be viewed online.)

strain highly focuses on the place above the middle of the sample before fracture as revealed in Fig. 5B, signifying an uneven distribution of strain under the external stress due to poor dispersion of MWCNTs within epoxy matrix. For the nano *g*-PS (0.0677 vol %)/epoxy, Fig. 5C, the major strain is also highly centered in the middle of the sample before fracture with a very thin layer as indicated by red. In comparison, in the nano *g*-PS (0.0677 vol %)/MWCNTs (0.0335 vol%)/epoxy nanohybrids, Fig. 5D, the highly concentrated major strain spreads most of dog-bone shaped sample before fracture, which suggests that more parts of samples tolerate the external stress arising from the uniform dispersion of nano *g*-PS and MWCNTs, further resulting in the enhanced mechanical properties. The 3D Motion and Deformation sensor ARAMIS system perfectly records the reinforcement process of nano *g*-PS (0.0677 vol%)/MWCNTs (0.0335 vol%)/epoxy nanohybrids and vividly demonstrates the enhancement mechanism by adding both nano *g*-PS and MWCNTs.

Based on the aforementioned SEM, TEM and 3D major strain distribution images analyses, the strengthening and toughening mechanism of nano *g*-PS/MWCNTs/epoxy nanohybrids is proposed. At the beginning, owing to the grafting chemical reaction (refer to supporiting materials: Scheme S1), the existence of epoxide and hydroxyl groups offers interfacial interaction between nano *g*-PS and epoxy matrix (the possible reaction is reported in our previous work [49]). Then MWCNTs tend to wrap outside the nano *g*-PS (because of the larger diameter of nano *g*-PS than that of MWCNTs) due to the high surface energy of both MWCNT and nano *g*-PS to achieve a better dispersion of the nanofillers within epoxy matrix. Finally, during the curing process at 120 °C, the nano *g*-PS transforms to fluid state, which allows nano *g*-PS polymers to flow into the voids between MWCNTs and epoxy matrix (that explains the fact that it's hard to see the nano *g*-PS particles in the SEM fracture images, Fig. 4E.) and serves as a bridge to stick MWCNTs and epoxy together, providing improved mechanical properties. The proposed mechanism is denoted in Fig. 6. This can also explains why our system exhibits a bigger improvement than other reported systems, Table 1. On one hand, the nano *g*-PS with the functional groups could help the dispersion of MWCNTs and increase the compatibility between nanofillers with epoxy; on the other hand, the MWCNTs without any chemical treatment could well maintain their original mechanical properties.

Lastly, as a character of antistatic properties [62], the surface resistivity of MWCNTs (0.0335 vol%)/epoxy nanocomposites and nano *g*-PS/MWCNTs (0.0335 vol%)/epoxy nanohybrids with different loadings of nano *g*-PS was measured. Similar to the volume resistivity (the reciprocal of electrical condutivity, Fig. S4), the

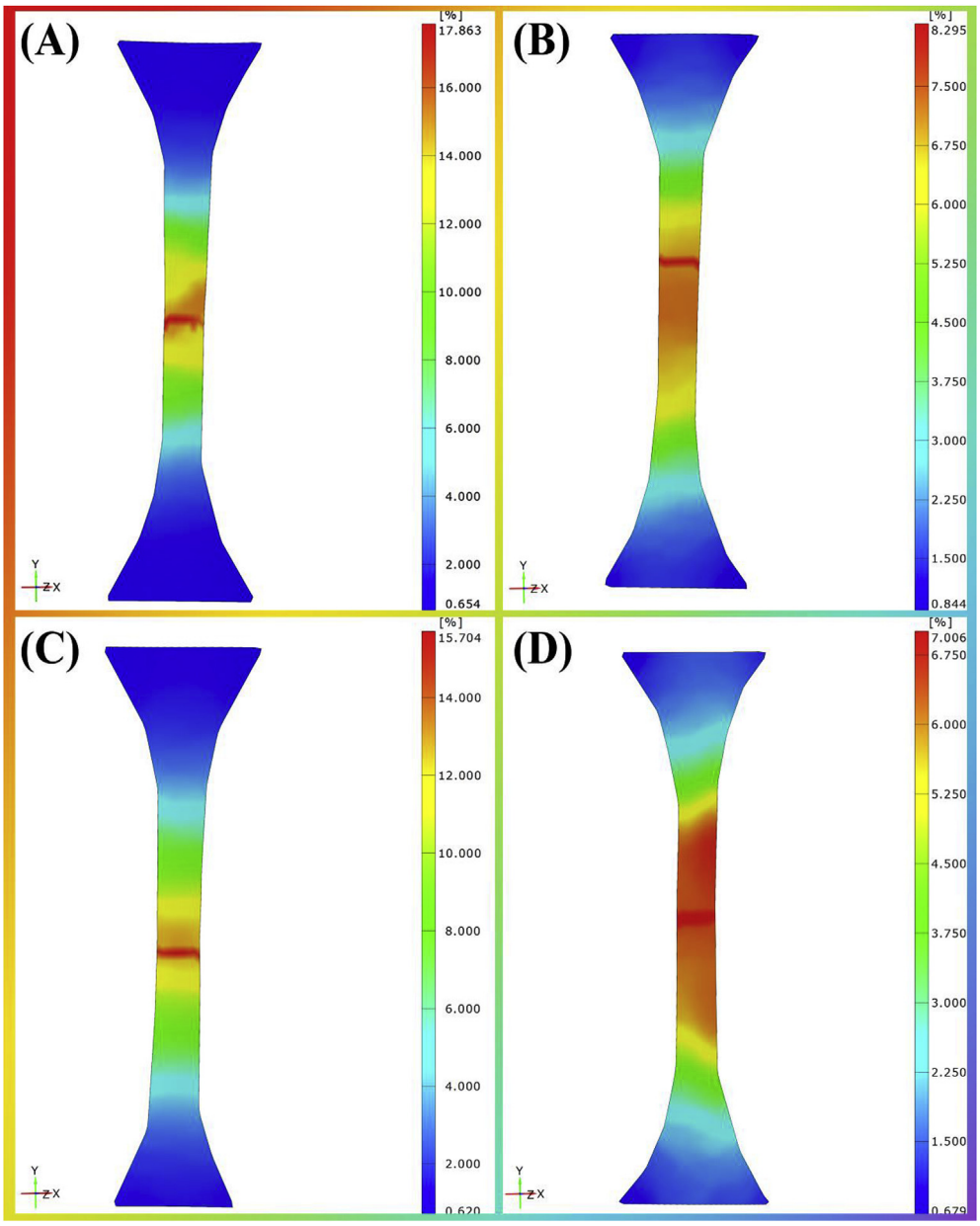

Fig. 5. 3D major strain distribution images of (A) pure epoxy, (B) MWCNTs (0.0335 vol%)/epoxy, (C) nano *g*-PS (0.0677 vol%)/epoxy,and (D) nano *g*-PS (0.0677 vol%)/MWCNTs (0.0335 vol%)/epoxy nanohybrids for the moment before fracture during the tensile process. (A colour version of this figure can be viewed online.)

surface resistivity reaches a lower value of $6.8 \times 10^4\ \Omega\ sq^{-1}$ as nano *g*-PS loading is 0.0677 vol%, which is one order of magnitude lower than that of MWCNTs (0.0335 vol%)/epoxy nanocomposites ($3.1 \times 10^5\ \Omega\ sq^{-1}$) because of better dispersion of MWCNTs in the nano *g*-PS/MWCNTs (0.0335 vol%)/epoxy nanohybrids as confirmed in the afromentioned parts, Fig. 7. Generally, sufficient antistatic properties can be achieved for a surface resistivity of materials in the range of $10^4 \sim 10^9\ \Omega\ sq^{-1}$ [63]. As the surface resistivity falls in this range, the lower surface resistivity, the higher antistatic properties will be acquired [64]. Our as-prepared nano *g*-PS/MWCNTs (0.0335 vol%)/epoxy nanohybrids possess a surface resistivity in the range of 6.8×10^4 to $2.0 \times 10^5\ \Omega\ sq^{-1}$, which is adequate for sufficient antistatic applications.

4. Conclusion

In summary, a strengthened and toughened epoxy nanohybrid had been prepared by simply mixing the electrosprayed nano *g*-PS particles with MWCNTs in the epoxy matrix. The presence of nano *g*-PS facilitated the dispersion of MWCNTs within epoxy and the synergies among nano *g*-PS, MWCNTs and epoxy matrix could efficiently destroy the entanglement of MWCNTs, causing the effective load transfer from week epoxy to the stronger nanofillers. The state transition of nano *g*-PS from glassy state to fluid state made nano *g*-PS flow into the void between MWCNTs and epoxy matrix, serving as a glue to tightly stick MWCNTs on the epoxy matrix, which contributed to the enhanced mechanical properties

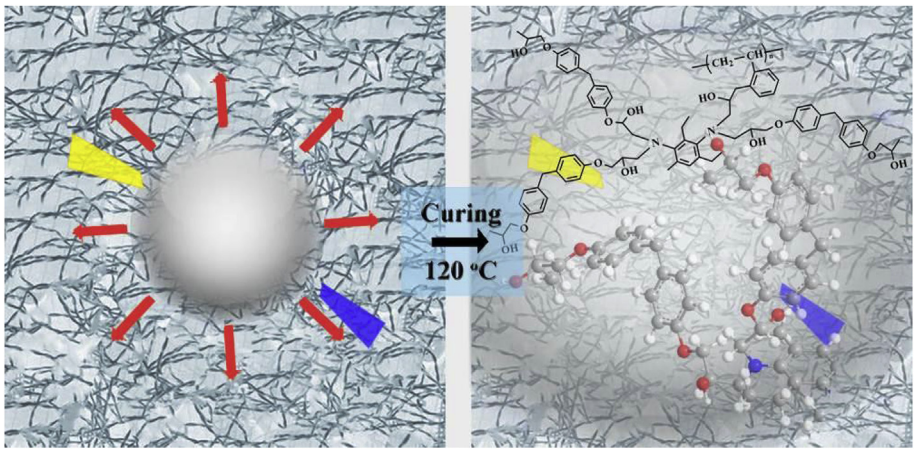

Fig. 6. Proposed mechanism for strengthening and toughening phenomenon in nano *g*-PS/MWCNTs/epoxy nanohybrids. (A colour version of this figure can be viewed online.)

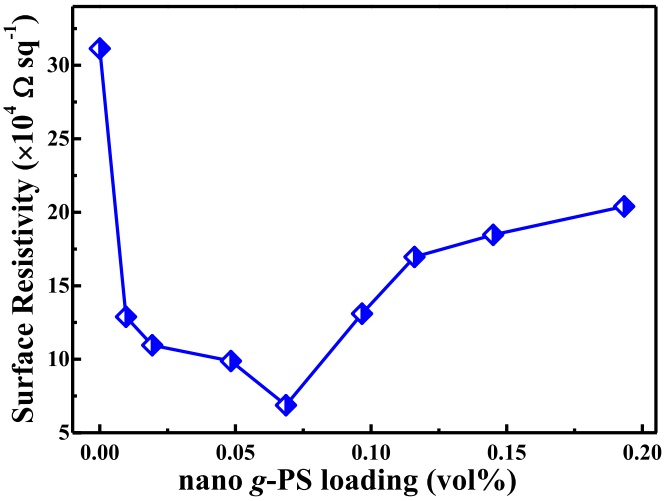

Fig. 7. Surface resistivity of nano *g*-PS/MWCNTs (0.0335 vol%)/epoxy nanohybrids. (A colour version of this figure can be viewed online.)

and increased electrical conductivity. Only 0.0677 vol% of nano *g*-PS and 0.0335 vol% loading of MWCNTs could significantly improve the tensile and flexural strength by 37.6 and 34.4%, respectively. In addition, these epoxy nanohybrids revealed an outstanding increase in tensile toughness by 279.2% and 108.3% increase in the elongation at break compared with pure epoxy. Compared with metals and ceramic materials [65–77], the decreased surface resistivity ($10^4\,\Omega$ sq^{-1}) enables nano *g*-PS/MWCNTs/epoxy nanohybrids for sufficient anti-static applications and potentially serve as the structural parts of aircraft fuselages to dissipate the lightning current and protect aircraft from the lightning strike.

Acknowledgement

This work is supported by Shanghai Science and Technology Commission (14DZ2261100). The authors thank for the support and funding from the Foundation of National Natural Science Foundation of China (No. 51703165), and Young Elite Scientists Sponsorship Program by CAST (YESS, No. 2016QNRC001).

Appendix A. Supplementary data

Supplementary data to this article can be found online at https://doi.org/10.1016/j.carbon.2018.10.029.

References

[1] H. Gu, C. Ma, J. Gu, J. Guo, X. Yan, J. Huang, Q. Zhang, Z. Guo, An overview of multifunctional epoxy nanocomposites, J. Mater. Chem. C 4 (2016) 5890–5906.
[2] C. Wang, M. Zhao, J. Li, J. Yu, S. Sun, S. Ge, X. Guo, F. Xie, B. Jiang, E.K. Wujcik, Y. Huang, N. Wang, Z. Guo, Silver nanoparticles/graphene oxide decorated carbon fiber synergistic reinforcement in epoxy-based composites, Polymer 131 (2017) 263–271.
[3] Y. He, S. Yang, H. Liu, Q. Shao, Q. Chen, C. Lu, Y. Jiang, C. Liu, Z. Guo, Reinforced carbon fiber laminates with oriented carbon nanotube epoxy nanocomposites: magnetic field assisted alignment and cryogenic temperature mechanical properties, J. Colloid Interface Sci. 517 (2018) 40–51.
[4] Z. Wu, S. Gao, L. Chen, D. Jiang, Q. Shao, B. Zhang, Z. Zhai, C. Wang, M. Zhao, Y. Ma, X. Zhang, L. Weng, M. Zhang, Z. Guo, Electrically insulated epoxy nanocomposites reinforced with synergistic core-shell Sio_2@MWCNTs and montmorillonite bifillers, Macromol. Chem. Phys. 218 (2017) 1700357.
[5] Y. Zhang, M. Zhao, J. Zhang, Q. Shao, J. Li, H. Li, B. Lin, M. Yu, S. Chen, Z. Guo, Excellent corrosion protection performance of epoxy composite coatings filled with silane functionalized silicon nitride, J. Polym. Res. 25 (2018) 130.
[6] Z. Hu, D. Zhang, F. Lu, W. Yuan, X. Xu, Q. Zhang, H. Liu, Q. Shao, Z. Guo, Y. Huang, Multistimuli-responsive intrinsic self-healing epoxy resin constructed by host-guest interactions, Macromolecules 51 (2018) 5294–5303.
[7] B. Song, T. Wang, H. Sun, H. Liu, X. Mai, X. Wang, L. Wang, N. Wang, Y. Huang, Z. Guo, Graphitic carbon nitride (g-C_3N_4) interfacially strengthened carbon fiber epoxy composites, Compos. Sci. Technol. 167 (2018) 515–521.
[8] B. Song, T. Wang, L. Wang, H. Liu, X. Mai, X. Wang, N. Wang, Y. Huang, Y. Ma, Y. Lu, E.K. Wujcik, Z. Guo, Interfacially reinforced carbon fiber/epoxy composite laminates via in-situ synthesized graphitic carbon nitride (g-C_3N_4), Composites Part B 158 (2019) 259–268.
[9] M. Zhao, L. Meng, L. Ma, L. Ma, X. Yang, Y. Huang, J.E. Ryu, A. Shankar, T. Li, C. Yan, Z. Guo, Layer-by-layer grafting CNTs onto carbon fibers surface for enhancing the interfacial properties of epoxy resin composites, Compos. Sci. Technol. 154 (2018) 28–36.
[10] A. Tsurumaki, S. Tajima, T. Iwata, B. Scrosati, H. Ohno, Antistatic effects of ionic liquids for polyether-based polyurethanes, Electrochim. Acta 175 (2015) 13–17.
[11] C. Liang, P. Song, H. Gu, C. Ma, Y. Guo, H. Zhang, X. Xu, Q. Zhang, J. Gu, Nanopolydopamine coupled fluorescent nanozinc oxide reinforced epoxy nanocomposites, Composites Part A 102 (2017) 126–136.
[12] H. Gu, S. Tadakamalla, Y. Huang, H.A. Colorado, Z. Luo, N. Haldolaarachchige, D.P. Young, S. Wei, Z. Guo, Polyaniline stabilized magnetite nanoparticle reinforced epoxy nanocomposites, ACS Appl. Mater. Interfaces 4 (2012) 5613–5624.
[13] Y. Liu, J. Zhao, L. Zhao, W. Li, H. Zhang, X. Yu, Z. Zhang, High performance shape memory epoxy/carbon nanotube nanocomposites, ACS Appl. Mater. Interfaces 8 (2016) 311–320.
[14] H. Du, C.X. Zhao, J. Lin, J. Guo, B. Wang, Z. Hu, Q. Shao, D. Pan, E.K. Wujcik, Z. Guo, Carbon nanomaterials in direct liquid fuel cells, Chem. Rec. 18 (2018) 1365–1372.
[15] K. Sun, P. Xie, Z. Wang, T. Su, Q. Shao, J. Ryu, X. Zhang, J. Guo, A. Shankar, J. Li, R. Fan, D. Cao, Z. Guo, Flexible polydimethylsiloxane/multi-walled carbon nanotubes membranous metacomposites with negative permittivity, Polymer 125 (2017) 50–57.
[16] Z. Li, B. Wang, X. Qin, Y. Wang, C. Liu, Q. Shao, N. Wang, J. Zhang, Z. Wang, C. Shen, Z. Guo, Superhydrophobic/superoleophilic polycarbonate/carbon nanotubes porous monolith for selective oil adsorption from water, ACS Sustain. Chem. Eng. (2018), https://doi.org/10.1021/acssuschemeng.1028b01637.
[17] Y. Lu, M.C. Biswas, Z. Guo, J.-W. Jeon, E.K. Wujcik, Recent developments in bio-

monitoring via advanced polymer nanocomposite-based wearable strain sensors, Biosens. Bioelectron. (2018), https://doi.org/10.1016/j.bios.2018.1008.1037.
[18] Y. Dong, J. Ding, J. Wang, X. Fu, H. Hu, S. Li, H. Yang, C. Xu, M. Du, Y. Fu, Synthesis and properties of the vapour-grown carbon nanofiber/epoxy shape memory and conductive foams prepared via latex technology, Compos. Sci. Technol. 76 (2013) 8–13.
[19] S. Zhai, L. Wei, H.E. Karahan, Y. Wang, C. Wang, A. Montoya, Q. Shao, X. Wang, Y. Chen, Ultrafast hydrothermal assembly of nanocarbon microfibers in near-critical water for 3D microsupercapacitors, Carbon 132 (2018) 698–708.
[20] R.K. Prusty, D.K. Rathore, S. Sahoo, V. Parida, B.C. Ray, Mechanical behaviour of graphene oxide embedded epoxy nanocomposite at sub- and above- zero temperature environments, Compos. Commun. 3 (2017) 47–50.
[21] J. Jia, X. Sun, X. Lin, X. Shen, Y.-W. Mai, J.-K. Kim, Exceptional electrical conductivity and fracture resistance of 3D interconnected graphene foam/epoxy composites, ACS Nano 8 (2014) 5774–5783.
[22] Y. Chen, H.B. Zhang, Y. Yang, M. Wang, A. Cao, Z.Z. Yu, High-performance epoxy nanocomposites reinforced with three-dimensional carbon nanotube sponge for electromagnetic interference shielding, Adv. Funct. Mater. 26 (2016) 447–455.
[23] G. Tang, Z.-G. Jiang, X. Li, H.-B. Zhang, S. Hong, Z.-Z. Yu, Electrically conductive rubbery epoxy/diamine-functionalized graphene nanocomposites with improved mechanical properties, Composites Part B 67 (2014) 564–570.
[24] P.-C. Ma, S.-Y. Mo, B.-Z. Tang, J.-K. Kim, Dispersion, interfacial interaction and re-agglomeration of functionalized carbon nanotubes in epoxy composites, Carbon 48 (2010) 1824–1834.
[25] M. Yoonessi, M. Lebrón-Colón, D. Scheiman, M.A. Meador, Carbon nanotube epoxy nanocomposites: the effects of interfacial modifications on the dynamic mechanical properties of the nanocomposites, ACS Appl. Mater. Interfaces 6 (2014) 16621–16630.
[26] H. Gu, S.B. Rapole, Y. Huang, D. Cao, Z. Luo, S. Wei, Z. Guo, Synergistic interactions between multi-walled carbon nanotubes and toxic hexavalent chromium, J. Mater. Chem. A 1 (2013) 2011–2021.
[27] B. Zhao, J. Deng, R. Zhang, L. Liang, B. Fan, Z. Bai, G. Shao, C.B. Park, Recent advances on the electromagnetic wave absorption properties of Ni based materials, Eng. Sci. 3 (2018) 5–40.
[28] Z.-Y. Zhou, N. Tian, J.-T. Li, I. Broadwell, S.-G. Sun, Nanomaterials of high surface energy with exceptional properties in catalysis and energy storage, Chem. Soc. Rev. 40 (2011) 4167–4185.
[29] M. Rahmat, P. Hubert, Carbon nanotube-polymer interactions in nanocomposites: a review, Compos. Sci. Technol. 72 (2011) 72–84.
[30] K.S. Khare, F. Khabaz, R. Khare, Effect of carbon nanotube functionalization on mechanical and thermal properties of cross-linked epoxy-carbon nanotube nanocomposites: role of strengthening the interfacial interactions, ACS Appl. Mater. Interfaces 6 (2014) 6098–6110.
[31] L.-J. Cui, H.-Z. Geng, W.-Y. Wang, L.-T. Chen, J. Gao, Functionalization of multi-wall carbon nanotubes to reduce the coefficient of the friction and improve the wear resistance of multi-wall carbon nanotube/epoxy composites, Carbon 54 (2013) 277–282.
[32] S.-Y. Yang, W.-N. Lin, Y.-L. Huang, H.-W. Tien, J.-Y. Wang, C.-C.M. Ma, S.-M. Li, Y.-S. Wang, Synergetic effects of graphene platelets and carbon nanotubes on the mechanical and thermal properties of epoxy composites, Carbon 49 (2011) 793–803.
[33] M. Li, Y. Gu, Y. Liu, Y. Li, Z. Zhang, Interfacial improvement of carbon fiber/epoxy composites using a simple process for depositing commercially functionalized carbon nanotubes on the fibers, Carbon 52 (2013) 109–121.
[34] J. Guo, H. Song, H. Liu, C. Luo, Y. Ren, T. Ding, M.A. Khan, D.P. Young, X. Liu, X. Zhang, J. Kong, Z. Guo, Polypyrrole-interface-functionalized nano-magnetite epoxy nanocomposites as electromagnetic wave absorbers with enhanced flame retardancy, J. Mater. Chem. C 5 (2017) 5334–5344.
[35] H. Gu, H. Zhang, C. Ma, S. Lyu, F. Yao, C. Liang, X. Yang, J. Guo, Z. Guo, J. Gu, Polyaniline assisted uniform dispersion for magnetic ultrafine barium ferrite nanorods reinforced epoxy metacomposites with tailorable negative permittivity, J. Phys. Chem. C 121 (2017) 13265–13273.
[36] R. Gulotty, M. Castellino, P. Jagdale, A. Tagliaferro, A.A. Balandin, Effects of functionalization on thermal properties of single-wall and multi-wall carbon nanotube-polymer nanocomposites, ACS Nano 7 (2013) 5114–5121.
[37] H. Gu, S. Tadakamalla, X. Zhang, Y.-D. Huang, Y. Jiang, H.A. Colorado, Z. Luo, S. Wei, Z. Guo, Epoxy resin nanosuspensions and reinforced nanocomposites from polyaniline stabilized multi-walled carbon nanotubes, J. Mater. Chem. C 1 (2013) 729–743.
[38] L. Liu, J.C. Grunlan, Clay assisted dispersion of carbon nanotubes in conductive epoxy nanocomposites, Adv. Funct. Mater. 17 (2007) 2343–2348.
[39] H. Gu, J. Guo, H. Wei, S. Guo, J. Liu, Y. Huang, A. Khan Mojammel, X. Wang, P. Young David, S. Wei, Z. Guo, Strengthened magnetoresistive epoxy nanocomposite papers derived from synergistic nanomagnetite-carbon nanofiber nanohybrids, Adv. Mater. 27 (2015) 6277–6282.
[40] Y. Lu, X. Gao, L. Jiang, Z. Chen, T. Wang, J. Jie, H. Kang, Y. Zhang, S. Guo, H. Ruan, Y. Zhao, Z. Cao, T. Li, Directly cast bulk eutectic and near-eutectic high entropy alloys with balanced strength and ductility in a wide temperature range, Acta Mater. 124 (2017) 143–150.
[41] D. Lee, S.H. Song, J. Hwang, S.H. Jin, K.H. Park, B.H. Kim, S.H. Hong, S. Jeon, Enhanced mechanical properties of epoxy nanocomposites by mixing non-covalently functionalized boron nitride nanoflakes, Small 9 (2013) 2602–2610.
[42] N. Domun, H. Hadavinia, T. Zhang, T. Sainsbury, G.H. Liaghat, S. Vahid, Improving the fracture toughness and the strength of epoxy using nanomaterials - a review of the current status, Nanoscale 7 (2015) 10294–10329.
[43] Y.T. Park, Y. Qian, C. Chan, T. Suh, M.G. Nejhad, C.W. Macosko, A. Stein, Epoxy toughening with low graphene loading, Adv. Funct. Mater. 25 (2015) 575–585.
[44] H. Zhu, S. Zhu, Z. Jia, S. Parvinian, Y. Li, O. Vaaland, L. Hu, T. Li, Anomalous scaling law of strength and toughness of cellulose nanopaper, Proc. Natl. Acad. Sci. Unit. States Am. 112 (2015) 8971–8976.
[45] B. Francis, V. Lakshmana Rao, S. Jose, B.K. Catherine, R. Ramaswamy, J. Jose, S. Thomas, Poly(ether ether ketone) with pendent methyl groups as a toughening agent for amine cured DGEBA epoxy resin, J. Mater. Sci. 41 (2006) 5467–5479.
[46] Z.J. Thompson, M.A. Hillmyer, J. Liu, H.-J. Sue, M. Dettloff, F.S. Bates, Block copolymer toughened epoxy: role of cross-link density, Macromolecules 42 (2009) 2333–2335.
[47] P.Y. Tae, Q. Yuqiang, C. Clement, S. Taewon, N.M. Ghasemi, W. M.C, S. Andreas, Epoxy toughening with low graphene loading, Adv. Funct. Mater. 25 (2015) 575–585.
[48] T. Sun, Z. Wu, Q. Zhuo, X. Liu, Z. Wang, H. Fan, Microstructure and mechanical properties of aminated polystyrene spheres/epoxy polymer blends, Composites Part A 66 (2014) 58–64.
[49] H. Gu, C. Ma, C. Liang, X. Meng, J. Gu, Z. Guo, A low loading of grafted thermoplastic polystyrene strengthens and toughens transparent epoxy composites, J. Mater. Chem. C 5 (2017) 4275–4285.
[50] H. Sun, X. Yang, Y. Zhang, X. Cheng, Y. Xu, Y. Bai, L. Shao, Segregation-induced in situ hydrophilic modification of poly (vinylidene fluoride) ultrafiltration membranes via sticky poly (ethylene glycol) blending, J. Membr. Sci. 563 (2018) 22–30.
[51] B. Xiang, D. Ling, H. Lou, H. Gu, 3D hierarchical flower-like nickel ferrite/manganese dioxide toward lead (II) removal from aqueous water, J. Hazard Mater. 325 (2017) 178–188.
[52] X. Yang, Z. Wang, L. Shao, Construction of oil-unidirectional membrane for integrated oil collection with lossless transportation and oil-in-water emulsion purification, J. Membr. Sci. 549 (2018) 67–74.
[53] H. Gu, H. Lou, J. Tian, S. Liu, Y. Tang, Reproducible magnetic carbon nanocomposites derived from polystyrene with superior tetrabromobisphenol A adsorption performance, J. Mater. Chem. A 4 (2016) 10174–10185.
[54] X. Jiang, S. Li, S. He, Y. Bai, L. Shao, Interface manipulation of CO_2-philic composite membranes containing designed UiO-66 derivatives towards highly efficient CO_2 capture, J. Mater. Chem. A 6 (2018) 15064–15073.
[55] H. Liu, M. Dong, W. Huang, J. Gao, K. Dai, J. Guo, G. Zheng, C. Liu, C. Shen, Z. Guo, Lightweight conductive graphene/thermoplastic polyurethane foams with ultrahigh compressibility for piezoresistive sensing, J. Mater. Chem. C 5 (2017) 73–83.
[56] H. Liu, Y. Li, K. Dai, G. Zheng, C. Liu, C. Shen, X. Yan, J. Guo, Z. Guo, Electrically conductive thermoplastic elastomer nanocomposites at ultralow graphene loading levels for strain sensor applications, J. Mater. Chem. C 4 (2016) 157–166.
[57] J.K.W. Sandler, J.E. Kirk, I.A. Kinloch, M.S.P. Shaffer, A.H. Windle, Ultra-low electrical percolation threshold in carbon-nanotube-epoxy composites, Polymer 44 (2003) 5893–5899.
[58] T.P. Sathishkumar, P. Navaneethakrishnan, S. Shankar, Tensile and flexural properties of snake grass natural fiber reinforced isophthallic polyester composites, Compos. Sci. Technol. 72 (2012) 1183–1190.
[59] H. Zhang, L.-C. Tang, Z. Zhang, K. Friedrich, S. Sprenger, Fracture behaviours of in situ silica nanoparticle-filled epoxy at different temperatures, Polymer 49 (2008) 3816–3825.
[60] J. Ma, M.-S. Mo, X.-S. Du, P. Rosso, K. Friedrich, H.-C. Kuan, Effect of inorganic nanoparticles on mechanical property, fracture toughness and toughening mechanism of two epoxy systems, Polymer 49 (2008) 3510–3523.
[61] R.O. Ritchie, The conflicts between strength and toughness, Nat. Mater. 10 (2011) 817–822.
[62] F.-L. Lou, Z.-J. Sui, J.-T. Sun, P. Li, D. Chen, X.-G. Zhou, Synthesis of carbon nanofibers/mica hybrids for antistatic coatings, Mater. Lett. 64 (2010) 711–714.
[63] T. Textor, B. Mahltig, A sol–gel based surface treatment for preparation of water repellent antistatic textiles, Appl. Surf. Sci. 256 (2010) 1668–1674.
[64] S. Araby, J. Li, G. Shi, Z. Ma, J. Ma, Graphene for flame-retarding elastomeric composite foams having strong interface, Composites Part A 101 (2017) 254–264.
[65] Z.-Y. Zhao, R.-G. Guan, J.-H. Zhang, Z.-Y. Zhao, P.-K. Bai, Effects of process parameters of semisolid stirring on microstructure of Mg-3Sn-1Mn-3SiC (wt %) strip processed by rheo-rolling, Acta Metall. Sin. (Eng. Lett.) 30 (2017) 66–72.
[66] Z. Zhao, P. Bai, R. Guan, V. Murugadoss, H. Liu, X. Wang, Z. Guo, Microstructural evolution and mechanical strengthening mechanism of Mg-3Sn-1Mn-1La alloy after heat treatments, Mater. Sci. Eng., A 734 (2018) 200–209.
[67] Y. Zhao, L. Qi, Y. Jin, K. Wang, J. Tian, P. Han, The structural, elastic, electronic properties and Debye temperature of D022-Ni3V under pressure from first-principles, J. Alloy. Comp. 647 (2015) 1104–1110.
[68] Y. Zhao, S. Deng, H. Liu, J. Zhang, Z. Guo, H. Hou, First-principle investigation of pressure and temperature influence on structural, mechanical and thermodynamic properties of Ti_3AC_2 (A = Al and Si), Comput. Mater. Sci. 154 (2018) 365–370.

[69] B. Song, T. Wang, H. Sun, Q. Shao, J. Zhao, K. Song, L. Hao, L. Wang, Z. Guo, Two-step hydrothermally synthesized carbon nanodots/WO3 photocatalysts with enhanced photocatalytic performance, Dalton Trans. 46 (2017) 15769–15777.
[70] C. Lin, L. Hu, C. Cheng, K. Sun, X. Guo, Q. Shao, J. Li, N. Wang, Z. Guo, Nano-$TiNb_2O_7$/carbon nanotubes composite anode for enhanced lithium-ion storage, Electrochim. Acta 260 (2018) 65–72.
[71] X. Lou, C. Lin, Q. Luo, J. Zhao, B. Wang, J. Li, Q. Shao, X. Guo, N. Wang, Z. Guo, Crystal structure modification enhanced FeNb11O29 anodes for lithium-ion batteries, ChemElectroChem 4 (2017) 3171–3180.
[72] Q. Hou, J. Ren, H. Chen, P. Yang, Q. Shao, M. Zhao, X. Zhao, H. He, N. Wang, Q. Luo, Z. Guo, Synergistic hematite-fullerene electron-extracting layers for improved efficiency and stability in perovskite solar cells, ChemElectroChem 5 (2018) 726–731.
[73] F. Liu, Z. Xu, Z. Wang, M. Dong, J. Deng, Q. Yao, H. Zhou, Y. Ma, J. Zhang, N. Wang, Z. Guo, Structures and mechanical properties of Nb-Mo-Co(Ru) solid solutions for hydrogen permeation, J. Alloy. Comp. 756 (2018) 26–32.
[74] W. Deng, T. Kang, H. Liu, J. Zhang, N. Wang, N. Lu, Y. Ma, A. Umar, Z. Guo, Potassium hydroxide activated and nitrogen doped graphene with enhanced supercapacitive behavior, Sci. Adv. Mater. 10 (2018) 937–949.
[75] H. Du, Y. An, Y. Wei, L. Hou, B. Liu, H. Liu, Y. Ma, J. Zhang, N. Wang, A. Umar, Z. Guo, Nickel powders modified nanocoating strengthened iron plates by surface mechanical attrition alloy and heat treatment, Sci. Adv. Mater. 10 (2018) 1063–1072.
[76] D. Pan, S. Ge, J. Zhao, Q. Shao, L. Guo, X. Zhang, J. Lin, G. Xu, Z. Guo, Synthesis, characterization and photocatalytic activity of mixed-metal oxides derived from NiCoFe ternary layered double hydroxides, Dalton Trans. 47 (2018) 9765–9778.
[77] D. Pan, S. Ge, X. Zhang, X. Mai, S. Li, Z. Guo, Synthesis and photoelectrocatalytic activity of In2O3 hollow microspheres via a bio-template route using yeast templates, Dalton Trans. 47 (2018) 708–715.
[78] M. Theodore, M. Hosur, J. Thomas, S. Jeelani, Influence of functionalization on properties of MWCNT-epoxy nanocomposites, Mater. Sci. Eng., A 528 (2011) 1192–1200.
[79] F.H. Gojny, M.H.G. Wichmann, B. Fiedler, K. Schulte, Influence of different carbon nanotubes on the mechanical properties of epoxy matrix composites – a comparative study, Compos. Sci. Technol. 65 (2005) 2300–2313.
[80] M. Naebe, J. Wang, A. Amini, H. Khayyam, N. Hameed, L.H. Li, Y. Chen, B. Fox, Mechanical property and structure of covalent functionalised graphene/epoxy nanocomposites, Sci. Rep. 4 (2014) 4375.
[81] Y. Ni, L. Chen, K. Teng, J. Shi, X. Qian, Z. Xu, X. Tian, C. Hu, M. Ma, Superior mechanical properties of epoxy composites reinforced by 3d interconnected graphene skeleton, ACS Appl. Mater. Interfaces 7 (2015) 11583–11591.
[82] Z. Wang, X. Shen, M. Akbari Garakani, X. Lin, Y. Wu, X. Liu, X. Sun, J.-K. Kim, Graphene aerogel/epoxy composites with exceptional anisotropic structure and properties, ACS Appl. Mater. Interfaces 7 (2015) 5538–5549.
[83] B. Ahmadi-Moghadam, M. Sharafimasooleh, S. Shadlou, F. Taheri, Effect of functionalization of graphene nanoplatelets on the mechanical response of graphene/epoxy composites, Mater. Des. 66 (2015) 142–149, 1980-2015.
[84] A. Mirmohseni, S. Zavareh, Preparation and characterization of an epoxy nanocomposite toughened by a combination of thermoplastic, layered and particulate nano-fillers, Mater. Des. 31 (2010) 2699–2706.
[85] A. A, K. L, V. L.R, N. N.K, Hydroxyl terminated poly(ether ether ketone) with pendant methyl group-toughened epoxy clay ternary nanocomposites: preparation, morphology, and thermomechanical properties, J. Appl. Polym. Sci. 106 (2007) 2936–2946.
[86] M. B, I. W, I. L, J. G, Property enhancement of epoxy resins by using a combination of polyamide and montmorillonite, Adv. Polym. Technol. 26 (2007) 223–231.